Multiresolution Regularized Least Squares Image Reconstruction Based on Wavelet in Optical Tomography

Wenwu Zhu*, Yao Wang*, Yining Deng*, Yuqi Yao* and Randall L. Barbour†

*Department of Electrical Engineering,
Polytechnic University , Brooklyn, NY 11201
†Departments of Pathology and Biophysics,
SUNY Health Science Center, Brooklyn, NY 11203

Abstract

In this paper, we present a wavelet based multigrid approach to solve the perturbation equation encountered in optical tomography. With this scheme, the unknown image, the data, as well as weight matrix are all represented by wavelet expansions, and thus yielding a multi-resolution representation of the original perturbation equation in the wavelet domain. This transformed equation is then solved using a multigrid scheme, by which an increasing portion of wavelet coefficients of the unknown image are solved in successive approximations. One can also quickly identify regions of interest (ROI) from a coarse level reconstruction and restrict the reconstruction in the following fine resolutions to those regions. At each resolution level, a regularized least squares solution is obtained using a Conjugate Gradient Descent (CGD) method. Compared to a previously reported one grid algorithm, the multigrid method requires substantially shorter computation time under the same reconstruction quality criterion.

1 Introduction

In this paper, we consider the recovery of optical properties in scattering media from continuous wave (CW) near infrared optical measurements. The problem is difficult because in this frequency range, photons propagate through the tissue in a highly diffused manner and the relation between the measured signal and the absorption properties of the media is non-linear. In the past few years, our group has developed an iterative perturbation approach for both CW, TR [1-3] and frequency domain data [4]. This requires the solution of a linear perturbation equation at each iteration:

$$\mathbf{Hx} = \mathbf{y}, \tag{1}$$

where $\mathbf{x}$ is an $N^2 \times 1$ vector of differences in the absorption properties between a reference and test medium, $\mathbf{y}$ an $M^2 \times 1$ vector of changes in detector readings between the two media, and $\mathbf{H}$ an $M^2 \times N^2$ matrix of weights describing the influence of each volume element (voxel) on the detector readings, which are essentially the derivatives of the detector readings with respect to the absorption coefficients in the reference medium. In general, the perturbation equation is both underdetermined and ill-posed. To solve the linear perturbation equation, several iterative algorithms have been developed, including projection onto convex sets (POCS) [1], CGD [1], multigrid reconstruction [1], layer stripping [2],[5] (for TR data), Regularized least squares (RLS) [5] [4], and total least squares (TLS) [6]. One challenging problem in solving the perturbation equation is that the computation complexity is usually very high due to the

0-8194-1929-X/95/$6.00

extremely large dimension of the weight matrix. In order to reduce the computation time, a wavelet based reconstruction algorithm is investigated in this paper. The unknown, the data and the weight matrix are expanded using wavelet, thus yielding a multi-resolution representation of the perturbation equation via wavelet transform. This transformed equation is solved from coarse to fine resolutions using the solution obtained from the previous resolution as the initial solution in the present resolution. The computational complexity is reduced significantly, compared to a one grid method which solves the equation in the finest resolution directly.

2 Wavelet Theory of Multiresolution Decomposition

2.1 1-D signal wavelet representation

Mallet [7] presented that any family of orthogonal wavelets can be used to generate multiresolution decomposition of a signal. Later on Unser [8] showed that any non-orthogonal wavelet family can also be use to decompose a signal, leading to the multiresolution representation. In this paper, we only consider the use of orthogonal wavelets. More specifically, we employ so called "discrete wavelets" which are obtained by binary dilations and dyadic translations of a "mother wavelet" $\psi(x)$, defined by

$$\psi_{j,k}(x) = 2^{j/2}\psi(2^j x - k), j, k \in \mathbf{Z}, \tag{2}$$

where $\mathbf{Z}$ is the set of all integers. In this wavelet family, j is a scale index while k is a location index. If $\psi(x)$ satisfies a certain condition, then $\psi_{j,k}, j, k \in \mathbf{Z}$ form a complete and orthogonal basis of $L^2(\mathbf{R})$, where $L^2(\mathbf{R})$ is the real function space with finite energy. For each $j \in \mathbf{Z}$, let W_j denote the closure of the linear span of $\psi_{j,k}, k \in \mathbf{Z}$, then $L^2(\mathbf{R})$ can be decomposed as an orthogonal sum:

$$L^2(\mathbf{R}) = \bigoplus_{j \in \mathbf{Z}} W_j, \tag{3}$$

where the circle around the plus sign indicates orthogonal sum.

Using wavelet series representation, any signal $f(x) \in L^2(\mathbf{R})$ can be represented as

$$f(x) = \sum_{j,k=-\infty}^{+\infty} c_{jk}\psi_{jk}(x), \tag{4}$$

where $c_{jk} = < f, \psi_{jk} >$, $< ., . >$ represents inner product.

For each $j \in \mathbf{Z}$, let us consider the closed subspaces

$$V_j = \ldots \oplus W_{j-1} \oplus W_j, j \in \mathbf{Z}, \tag{5}$$

of $L^2(\mathbf{R})$. It can be shown that V_j is the linear span of scaling functions $\phi_{j,k}(x) = 2^{j/2}\phi(2^j x - k), j, k \in \mathbf{Z}$, where $\phi(x)$ has "two-scale relations" with wavelet $\psi(x)$ given by

$$\phi(x) = \sum_k p_k \phi(2x - k); \quad \psi(x) = \sum_k q_k \phi(2x - k), \tag{6}$$

where p_k and q_k are a pair of QMF (Quadrature Mirror Filters) and $q_k = (-1)^{1-k} p_{(k-1)}$.

The subspace V_j and W_j satisfy the following relation

$$V_j = V_{j-1} \oplus W_{j-1}, j \in \mathbf{Z} \tag{7}$$

$$= V_{j-L} \oplus W_{j-L} \oplus W_{j-L-1} \oplus \ldots \oplus W_{j-1}. \tag{8}$$

Correspondingly, any $f_j \in V_j$ has a unique decomposition:

$$f_j = f_{j-1} + g_{j-1}, j \in \mathbf{Z} \quad (9)$$

$$= f_{j-L} \oplus g_{j-L} \oplus g_{j-L-1} \oplus \cdots \oplus g_{j-1}, \quad (10)$$

where $f_j \in V_j$ and $g_j \in W_j$. This is usually called wavelet decomposition of f_j, where

$$f_j = \sum_{k=-\infty}^{+\infty} c_k^j \phi_{j,k}(x), \qquad c_k^j = < f_j, \phi_{j,k}(x) >,$$

$$g_j = \sum_{k=-\infty}^{+\infty} d_k^j \psi_{j,k}(x), \qquad d_k^j = < f_j, \psi_{j,k}(x) > . \quad (11)$$

Eq. (9) implies that a signal at scale j can be decomposed to an "approximation signal" at the next scale f_{j-1} and "detail signal" g_{j-1}. This can be implemented by QMF in practice, where f_{j-1} and g_{j-1} are low frequency output and high frequency output, respectively. Eq.(10), on the other hand, provides a multiresolution representation of f_j, by an approximation signal f_{j-L} at the coarsest resolution, plus detailed signals at increasing scales.

For a discrete signal with N samples, the wavelet transform can be represented in the following matrix form:

$$\tilde{\mathbf{f}} = \mathbf{W}\mathbf{f}. \quad (12)$$

In Eq. (12), $\mathbf{f} = [f(x_1), f(x_2), ..., f(x_N)]^T = [f_1, f_2, ..., f_N]^T$ consists of the discrete sample of the original signal, $\tilde{\mathbf{f}} = [\tilde{f}_1, \tilde{f}_2, ..., \tilde{f}_N]^T$ consists of the wavelet transform coefficients, including c_k^j and d_k^j, and $\mathbf{W}$ is an $N \times N$ matrix. The elements of $\mathbf{W}$ depends on the samples of the scaling and wavelet functions, $\phi_{jk}(x_i)$, $\psi_{jk}(x_i)$.

2.2 2-D signal wavelet representation

In general, a 2D image can be arranged into a vector by lexicographic order. The 1D wavelet transform described before can then be applied to the vector. One can then reorder the vector to a 2D image. However, a more efficient way of implementing a wavelet transform of a 2D image is by applying a 1D transform to each rows of the 2D image first, and then applying a 1D wavelet transform to each column. This is known as separable wavelet transform. Using a separable scaling function $\phi(x,y) = \phi(x)\phi(y)$ and separable wavelets $\psi_{lh}(x,y) = \phi(x)\psi(y), \psi_{hl}(x,y) = \psi(x)\phi(y), \psi_{hh}(x,y) = \psi(x)\psi(y)$, where $\psi(x)$ is the 1-D wavelet associated with 1-D scaling function $\phi(x)$, we can decompose an image $f(x,y) \in V_j$ in $L^2(\mathbf{R^2})$ into four subimages consisting of approximation image $A_{j-1}f$ and three detail subimages $D_{j-1}^1 f$, $D_{j-1}^2 f$ and $D_{j-1}^3 f$. This can be implemented by a set of QMFs illustrated in Fig. 1 (2-levels). Usually we refer them as LL, LH, HL and HH images, respectively, from top to bottom. One can continue to decompose the subimage $A_{j-1}f$ further to the next scale (coarser resolution) leading to a pyramid structure. The L level MRA representation of an image is given by

$$f = A_0 f = A_{-L} f + \sum_{i=-1}^{-L} D_i f. \quad (13)$$

Let $\mathbf{X}$ represent the 2D image with size $N \times N$, and let $\mathbf{x}$ be the vector consisting of elements of $\mathbf{X}$ arranged in the lexicographic order, with size N^2. Let $\mathbf{W_x}$ represent the 1D wavelet transform matrix of size $N \times N$, the separable wavelet transform of $\mathbf{X}$ can be described by:

$$\tilde{\mathbf{X}} = \mathbf{W_x}\, \mathbf{X}\, \mathbf{W_x}^T, \quad (14)$$

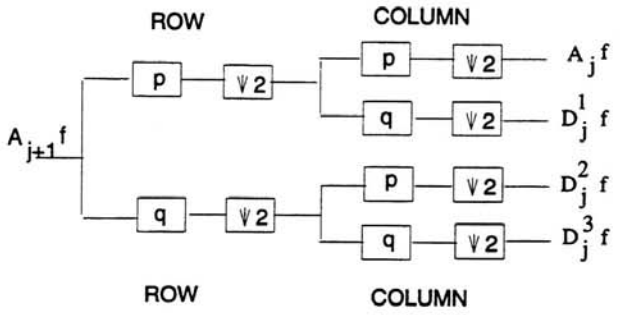

Figure 1: Wavelet decomposition of 2D image from level $j+1$ to j

where T denotes transpose. This is equivalent to, in the 1D notation,

$$\tilde{\mathbf{x}} = (\mathbf{W_x} \otimes \mathbf{W_x})\,\mathbf{x}, \tag{15}$$

where $\otimes$ denotes the Kronecker product, and $\tilde{\mathbf{x}}$ is the vector consisting of elements of $\tilde{\mathbf{X}}$ arranged in the lexicographic order. Therefore, performing 2D wavelet transform to 2D image using separable transform matrix $\mathbf{W_x}$ is equivalent to performing the wavelet transform to the corresponding 1D vector by using $\mathbf{W}_{N^2} = \mathbf{W_x} \otimes \mathbf{W_x}$.

3 Solution of the Pertubation Equation in the Wavelet Domain

3.1 1-D wavelet representation of the perturbation equation

Considering the perturbation equation in Eqn. (1). To represent the perturbation equation in a wavelet domain, let the transform matrices for $\mathbf{x}$ and $\mathbf{y}$ be represented by $\mathbf{W_x}$ and $\mathbf{W_y}$, respectively. Multiplying Eq. (1) from left by $\mathbf{W_y}$ and inserting $\mathbf{W_x}^T\mathbf{W_x} = \mathbf{I}$ in between $\mathbf{H}$ and $\mathbf{x}$, we obtain:

$$\tilde{\mathbf{H}}\,\tilde{\mathbf{x}} = \tilde{\mathbf{y}}\,. \tag{16}$$

where $\tilde{\mathbf{H}} = \mathbf{W_y}\mathbf{H}\mathbf{W_x}^T$, $\tilde{\mathbf{y}} = \mathbf{W_y}\mathbf{y}$ and $\tilde{\mathbf{x}} = \mathbf{W_x}\mathbf{x}$. Here we assume the transform matrices are orthogonal so that $\mathbf{W_y}^T\mathbf{W_y} = \mathbf{I}$. Eq. (16) is the perturbation equation in the wavelet domain. From this equation, one can solve $\hat{\tilde{\mathbf{x}}}$, the wavelet transform of $\hat{\mathbf{x}}$. One can then obtain $\hat{\mathbf{x}}$ by an inverse transform $\hat{\mathbf{x}} = \mathbf{W_x}^T\,\hat{\tilde{\mathbf{x}}}$.

3.2 Regularized least squares (RLS) solution in wavelet domain

Regularization is a well-established technique for dealing with instability in inverse problems [10] and can convert an ill-posed problem into a well-posed problem by incorporating *a priori* knowledge about the image to be recovered. Regularized Least Squares (RLS) can be formulated as

$$\hat{\mathbf{x}} = \arg\min_{\mathbf{x}}\{\|\mathbf{H}\mathbf{x} - \mathbf{y}\|^2 + \lambda\|\mathbf{x}\|^2\}, \tag{17}$$

where the *regularization parameter* λ can be determined by the Miller criterion [11] or Cross-validation method [12]. The regularized solution is given by

$$\hat{\mathbf{x}} = (\mathbf{H}^T\mathbf{H} + \lambda\mathbf{I})^{-1}\mathbf{H}^T\mathbf{y}. \tag{18}$$

In the wavelet domain, the RLS can be formulated as

$$\hat{\tilde{\mathbf{x}}} = \arg\min_{\tilde{\mathbf{x}}}\{\|\tilde{\mathbf{H}}\tilde{x} - \tilde{y}\|^2 + \lambda\|\tilde{\mathbf{x}}\|^2\}, \tag{19}$$

with corresponding solution given by

$$\hat{\tilde{\mathbf{x}}} = (\tilde{\mathbf{H}}^T\tilde{\mathbf{H}} + \lambda\mathbf{I})^{-1}\tilde{\mathbf{H}}^T\tilde{\mathbf{y}}. \tag{20}$$

3.3 2-D separable wavelet representation

Suppose $\mathbf{x}$ and $\mathbf{y}$ in Eq. (1) are vectors obtained from 2D $N \times N$ image $\mathbf{X}$ and $M \times M$ image $\mathbf{Y}$ in the lexicographic order. Let $\mathbf{W_x}$ and $\mathbf{W_y}$ represent 1D transform matrices for $\mathbf{X}$ and $\mathbf{Y}$, respectively. Define $\mathbf{W}_{M^2} = \mathbf{W_y} \otimes \mathbf{W_y}$ and $\mathbf{W}_{N^2}^T = \mathbf{W_x}^T \otimes \mathbf{W_x}^T$, then similar to the 1D case, we have

$$\tilde{\mathbf{H}} = \mathbf{W}_{M^2}\mathbf{H}\mathbf{W}_{N^2}{}^T, \quad \tilde{\mathbf{y}} = \mathbf{W}_{M^2}\mathbf{y}, \quad \tilde{\mathbf{x}} = \mathbf{W}_{N^2}\mathbf{x}. \tag{21}$$

Substituting $\tilde{\mathbf{H}}, \tilde{\mathbf{y}}$, and $\tilde{\mathbf{x}}$ into Eqn.(20), we can have the RLS solution in the 2D wavelet domain. The question is how to calculate the 4D wavelet transform $\tilde{\mathbf{H}} = \mathbf{W}_{M^2}\mathbf{H}\mathbf{W}_{N^2}{}^T$. Slightly different from [13], we do the following. First, for each row $\mathbf{h}_{r_i}$, $i = 1, 2, ..., M^2$ of $\mathbf{H}$, we reorder it to a 2D image of size $N \times N$ and then use $\mathbf{W}_x$ to perform separable transform. After transforming each row, we reorder the transformed image back to a row vector $\tilde{\mathbf{h}}_{r_i}$. Let the resulting image be $\tilde{\mathbf{H}}_r = \mathbf{H}\mathbf{W}_{N^2}^T$. Then, for each column of $\tilde{\mathbf{H}}_r$, $\tilde{\mathbf{h}}_{c_j}$, $j = 1, 2, ..., N^2$, we perform $\mathbf{W}_{M^2}\,\tilde{\mathbf{h}}_{c_j}$ in the form of $\mathbf{W_y}(\tilde{\mathbf{H}}_{c_j})_{2D}\mathbf{W_y}$ $j = 1, 2, ..., N^2$, where $(\tilde{\mathbf{H}}_{c_j})_{2D}$ is the 2D ordering of $(\tilde{\mathbf{h}}_{c_j})$. Finally we reorder the transformed vectors to a 2D matrix which is $\tilde{\mathbf{H}}$.

4 Multigrid Algorithm

As we see from section 2, wavelet decomposition of a signal leads to a multiresolution representation of the signal. If we exploit the multiresolution property, the computational time will be reduced. In this paper, we use a modified V-cycle algorithm. The principle of this algorithm is illustrated in Fig. 2. There are two differences compared to the classical V-cycle method [14]. First, instead of downward (from fine to coarse) restriction where error is calculated and restricted, here we use wavelet decomposition to reach the vertex (coarsest grid) of the V-cycle. For the upward reconstruction (form coarse to fine), we use multigrid reconstruction instead of error prolongation (error compensation). Specifically, this modified V-cycle algorithm consists of the following steps:

1. Perform wavelet transform of $\mathbf{y}$ and $\mathbf{H}$ to obtain $\tilde{\mathbf{H}}_l$ and $\tilde{\mathbf{y}}_l$, $l = -1, -2, ..., -L$. Set $l = -L$.
2. Solve for the RLS solution $\hat{\tilde{\mathbf{x}}}_l$ of the perturbation equation at the lth level, $\tilde{\mathbf{H}}_l\tilde{\mathbf{x}}_l = \tilde{\mathbf{y}}_l$ using the CGD algorithm.
3. Prolongate from $\tilde{\mathbf{x}}_l$ to $\tilde{\mathbf{x}}_{l+1}$ by padding zeros, i.e., $\tilde{\mathbf{x}}_{l+1} = [\tilde{\mathbf{x}}_l^T,\ \mathbf{0}]^T$.
4. Let $l = l + 1$, if $l = 0$ stop, otherwise, go back to 2.

The wavelet based multigrid RLS algorithm described above slightly differs from the one proposed by Wang et al. [15] in several aspects. First, in that method, at each resolution level, the LL, LH, HL and HH components are reconstructed alternatingly until the solution converges. In our method, at each level, the LL component only is solved, assuming the other components are zeros. Secondly, in the method of [15], the regularization parameter is fixed at a constant at different resolutions. In our multigrid RLS, the regularization parameters at different grids (resolutions) are varied. In the coarsest resolution, the noise is quite weak, so we do not need to apply much regularization. When the resolution goes from coarse to fine, the regularization parameter is increased. This is because the noise is more pronounced in high frequencies.

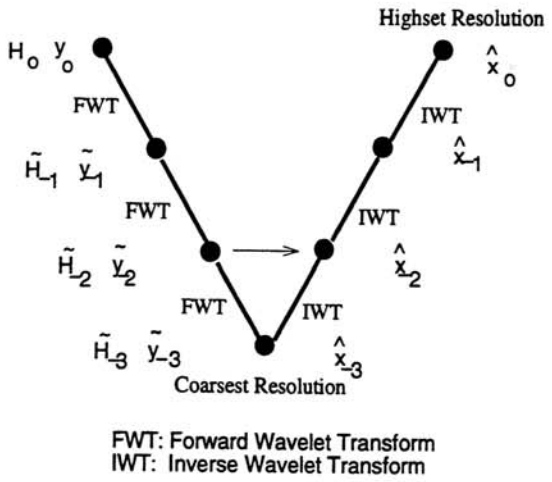

Figure 2: Modified V-cycle multigrid algorithm

In real clinic applications, most of time one is only interested in certain regions with abnormal features. The above multigrid algorithm can not only save computational time compared to the one-grid algorithm, but also allow one to "zoom-in" special regions of interests (ROI). Let's say we are interested in a region that appears "questionable" in a coarser level reconstruction. Then only the corresponding region in the next finer resolution need to be further refined by the CGD algorithm, while other regions can be kept as the result obtained in the previous coarser resolution.

Currently, we have only implemented a two-grid algorithm ($L = 1$) by which we first reconstruct the LL component of the wavelet transform $\tilde{\mathbf{x}}$ of $\mathbf{x}$. This yields the coarse level reconstruction $\tilde{\mathbf{x}}_{-1}$. Starting from this solution, we then solve all the components of $\tilde{\mathbf{x}}$.

5 Experimental Results

In order to demonstrate the effectiveness of the wavelet based multigrid RLS algorithm compared to a one-grid algorithm, two sets of experiments are performed. In the first experiment, a $1cm$ diameter rod is placed in an infinite homogeneous medium. The rod is homogeneous, with absorption and scattering coefficients $\mu_a = 0.05cm^{-1}$ and $\mu_s = 10cm^{-1}$. The background medium has $\mu_a^b = 0.02cm^{-1}$ and $\mu_s^b = 10cm^{-1}$. A total of 16 sources and 16 detectors are evenly spread about the rod in a ring geometry having a diameter of 10 cm. Solution to the forward problem was accomplished by analytically solving the diffusion equation using the normal mode series method described in reference [17]. Fig. 3 shows the comparison of the reconstructed images using one-grid and two-grid algorithms, respectively. The coarse level reconstruction only solves a quarter of the pels in the fine resolution. In our computer implementation, one iteration of the coarse level roughly requires 1/7 of the computational time taken by one iteration in the fine resolution. From the experimental results, we see that the proposed multigrid algorithm can obtain significantly better reconstruction than the one-grid method under similar computation time, or require significantly shorter time to reach the same resolution quality. In the second experiment, a $1.5cm$ diameter rod is placed at an off-center position with respect to the source and detector ring. The rod has a nonhomogeneous absorption distribution, following a sinusoidal pattern (one positive cycle only). The forward solution in this experiment is obtained by a multigrid finite difference solver described in [4]. Fig. 4 is the reconstruction

results of the off-center case. We also show the wavelet decomposition of the original image and the final reconstructed image. From this figure, we can see that we can obtain quite accurate results from the coarse level reconstruction alone, in this example. This is because the energy of the original image is mostly contained in the LL band. This energy compaction property of the wavelet transform makes the reconstruction in the wavelet domain more efficiently for images that are smooth.

In the above examples, the calculated data from the forward solution were used and the regularization parameter was set to zero. Below, we show the results when the data are corrupted by 10% white Gaussian noise, with an equivalent signal to noise ratio (SNR) of 20 dB. Fig. 5 compares the reconstruction results with and without regularization in each grid. The regularization parameter was chosen roughly based on the Miller criterion, followed by slight manual tuning. The regularization parameter in the coarse grid is one magnitude smaller than that in the fine grid. From these results, we can see that the use of regularization is more efficient in the fine grid (compare (c) and (e)). Further we also see that if we impose regularization in both coarse grid and fine grid we can always get better reconstruction in each grid.

6 Conclusion and Discussion

In this paper, a wavelet based multiresolution RLS reconstruction scheme is proposed for solving the perturbation equation. The proposed scheme performs reconstruction in the wavelet domain using a multigrid algorithm. At each grid level, a CGD algorithm is used to obtain the RLS solution of the perturbation equation at that grid. It can achieve substantial computational savings compared to the one-grid method. The incorporation of regularization in the wavelet domain can suppress noise effectively. This scheme also enables one to focus on regions of interest (ROI) from coarse to fine resolution.

7 Acknowledgement

This work was supported in part by the National Institutes of Health under Grant # RO1-CA59955, by an ONR grant # N000149510063, and by the New York State Science and Technology Foundation.

References

[1] Y. Wang, J. Chang, R. Aronson, R.L. Barbour, H.L. Graber, and J. Lubowsky, "Imaging scattering media by diffusion tomography: An iterative perturbation approach," in *Proc. Physiological Monitoring and Early Detection Diagnostic Methods*, vol. SPIE-1641, (Los Angeles), pp. 58–71, Jan. 1992.

[2] J. Chang, Y. Wang, R. Aronson, H. L. Graber, and R.L. Barbour, "A layer-stripping approach for recovery of scattering media from time-resolved data," in *Proc. Inverse Problems in Scattering and Imaging*, vol. SPIE–1767, (San Diego), pp. 384–395, July 1992.

[3] R. L. Barbour, H. L. Graber, Y. Wang, J. Chang, and R. Aronson, "A perturbation approach for optical diffusion tomography using continuous-wave and time-resolved data," *SPIE Medical Optical Tomography — Functional Imaging and Monitoring*, SPIE Institutes, IS11, pp. 87-120, 1993.

[4] Y. Q. Yao, Y. Wang, Y. L. Pei, W. W. Zhu, J. H. Hu and R. L. Barbour, " Frequency Domain Optical Tomography In Human Tissue," *in this proceedings.*

[5] W. Zhu, Y. Wang, H. L. Graber, R. L. Barbour and J. Chang, "A Regularized Progressive Expansion Algorithm for Recovery of Scattering Media from Time-Resolved Data," in *Advances in Optical*

Imaging and Photon Migration , pp.211-216, edited by Robert R. Alfano, Optical Society of America, 1994.

[6] W. Zhu, Y. Wang, J. Chang, H. L. Graber, and R. Barbour, "A Total Least Squares approach for the solution of the perturbation equation," in *Proc. of Optical Tomography, Photon Migration, and Spectroscopy of Tissue and Model Media,* part of *An International Symposium on Biomedical optics,* pp.420-430, SPIE vol. 2389, San Jose, Feb. 1995.

[7] S. G. Mallet, "A theory for multiresolution signal decomposition: The wavelet representation," *IEEE Trans. on Pattern Anal. Machine intell.*, vol. 11, no. 7 , pp.674-693, 1989.

[8] M. Unser, A. Aldroubi, and M. Eden, "A family of polynomial spline wavelet transform", *Signal Processing*, vol. 30, no.2, pp. 141-162, 1993.

[9] J. Kovacevic and M. Vetterli, "Nonseparable multidimensional perfect reconstruction filter banks and wavelet basis for $\mathbf{R_n}$,"

[10] A. N. Tikhonov and V. Y. Arsenin, *Solution of Ill-Posed Problems*, Washington D. C.: V. H. Winston, 1977.

[11] K. Miller, "Least squares method for ill–posed problems with a prescribed bound," *SIAM J. of Mathematical Analysis,* vol. 1, pp. 52–74, Feb. 1970.

[12] G. H. Golub, M. Heath, and G. Wahba, "Generalized cross-validation as a method for choosing a good ridge parameter," *Technometrics*, vol. 21, No. 2, pp. 215-223, 1979.

[13] L. Blanc-Feraud, P. Charbonnier, P. Lobel and M. Barlaud, "A fast tomographic reconstruction algorithm in the 2D wavelet transform domain," in *Proc. IEEE Int Conf. ASSP (ICASSP94),* vol. V, pp. 305–308.

[14] W. Hackbusch, *Multigrid Methods and Applications*, Berlin: Springer-Verlag, 1985.

[15] G. Wang, J. Zhang and G. W. Pan, "Solution of inverse problems in image processing by wavelet expansion," *IEEE Trans. on Image Processing*, vol. 4, no. 5, pp. 579-593.

[16] A. H. Delaney and Y. Bresler, "Multiresolution tomographic reconstruction using wavelets," to appear in *IEEE Trans. on Image Processing*, 1995.

[17] Y. Q. Yao, Y. Wang, R. L. Barbour, H. L. Graber and J. W. Chang, "Scattering Characteristics of Photon Density Waves from an Object in a Spherically Two-Layer Medium," *In SPIE Proceedings on Biomedical Optics*, B. Chance and R. R. Alfano, ed., Vol. 2389, pp. 291-303, (1995).

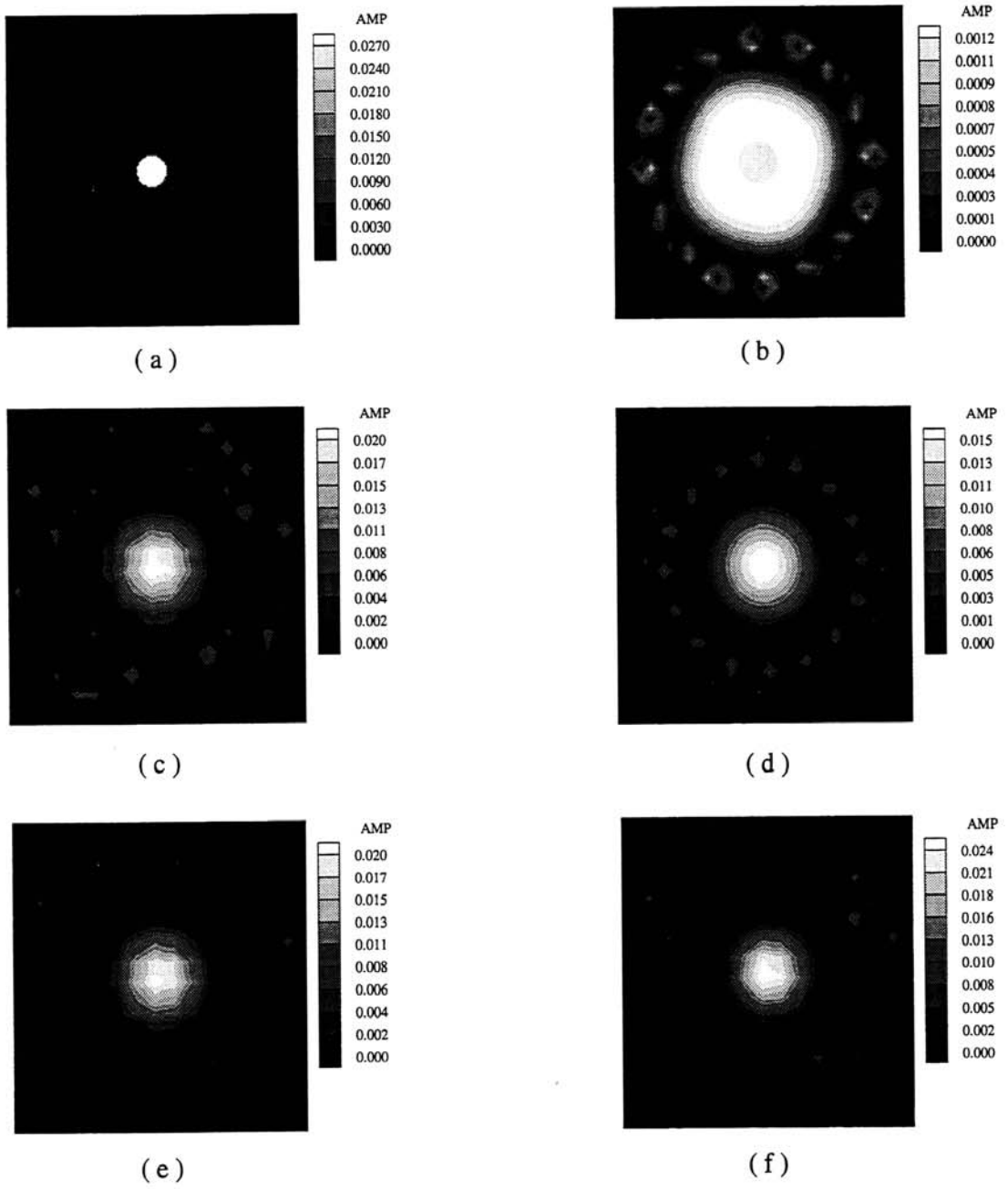

Figure 3: Reconstructed results for a medium with a centered rod. (a) is the original image. (b) is the reconstructed image using one-grid CGD with 32 iterations; (c) is the reconstructed image using two-grid algorithm with 500 iterations in the coarse grid; (d) is the reconstructed image using one grid CGD with 235 iterations; (e) is the reconstructed image using the two-grid algorithm with additional 200 iterations in the fine grid, using (c) as initial solution; and (f) is the reconstructed image with 800 iterations in a localized region at the fine grid, also using (c) as the initial solution. The computation time for (b) and (c) are roughly same. So are (d), (e) and (f). The time for (c) is about 1/7 of (d).

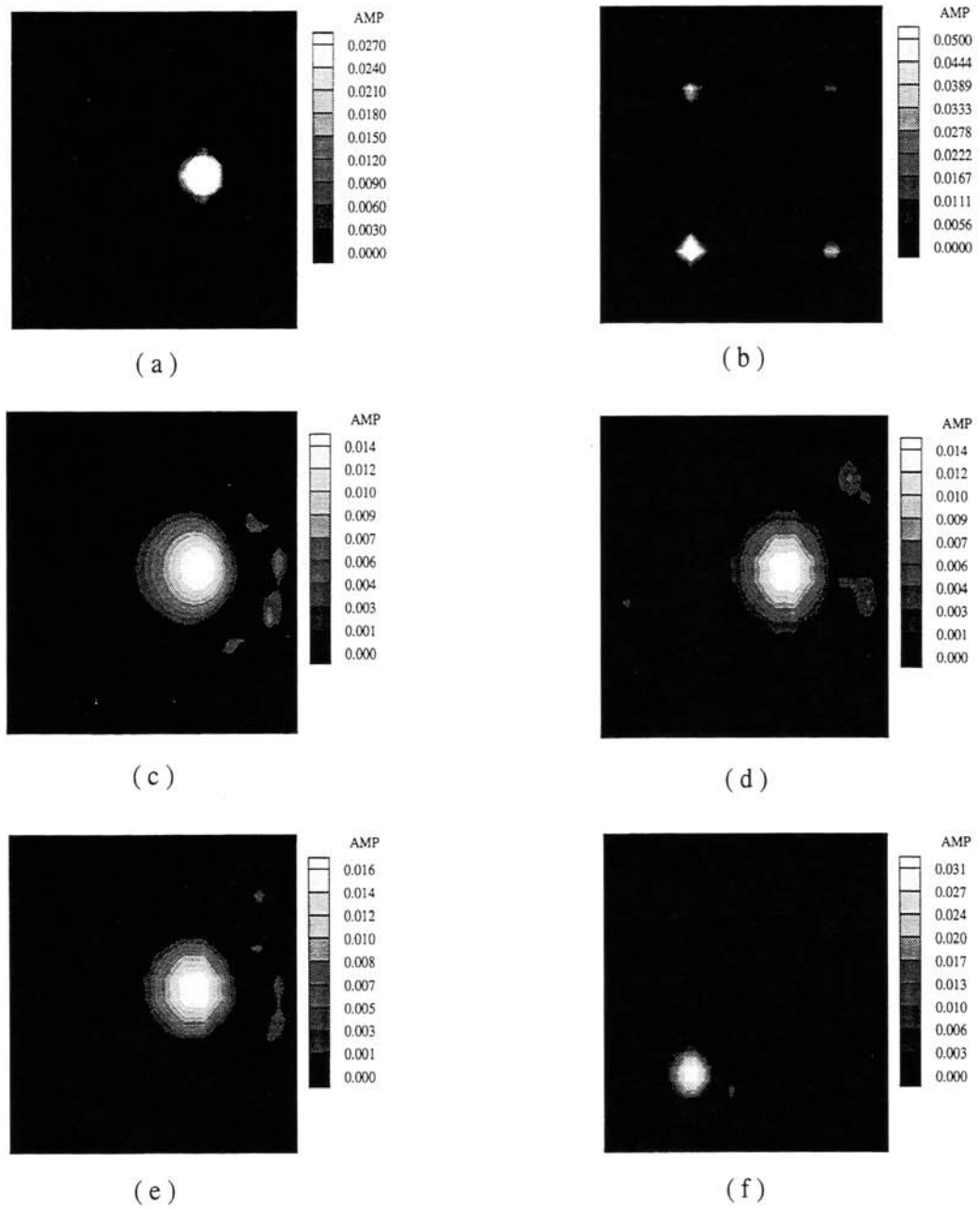

Figure 4: Reconstruction results and wavelet analysis of a medium with an off-center rod with Sin-like distribution. (a) is the original image; (b) shows the wavelet transform of original image in (a); (c) is the reconstruction result using one grid with 235 iterations; (d) is the reconstruction image using two-grids algorithm with 500 iterations in the coarse grid; (e) is the reconstruction image using two-grid algorithm with additional 200 iterations in the fine grid; and (f) is the wavelet transform of (e). The total computation time for (e) and (c) are roughly the same. The time for (d) is about 1/7 of (c).

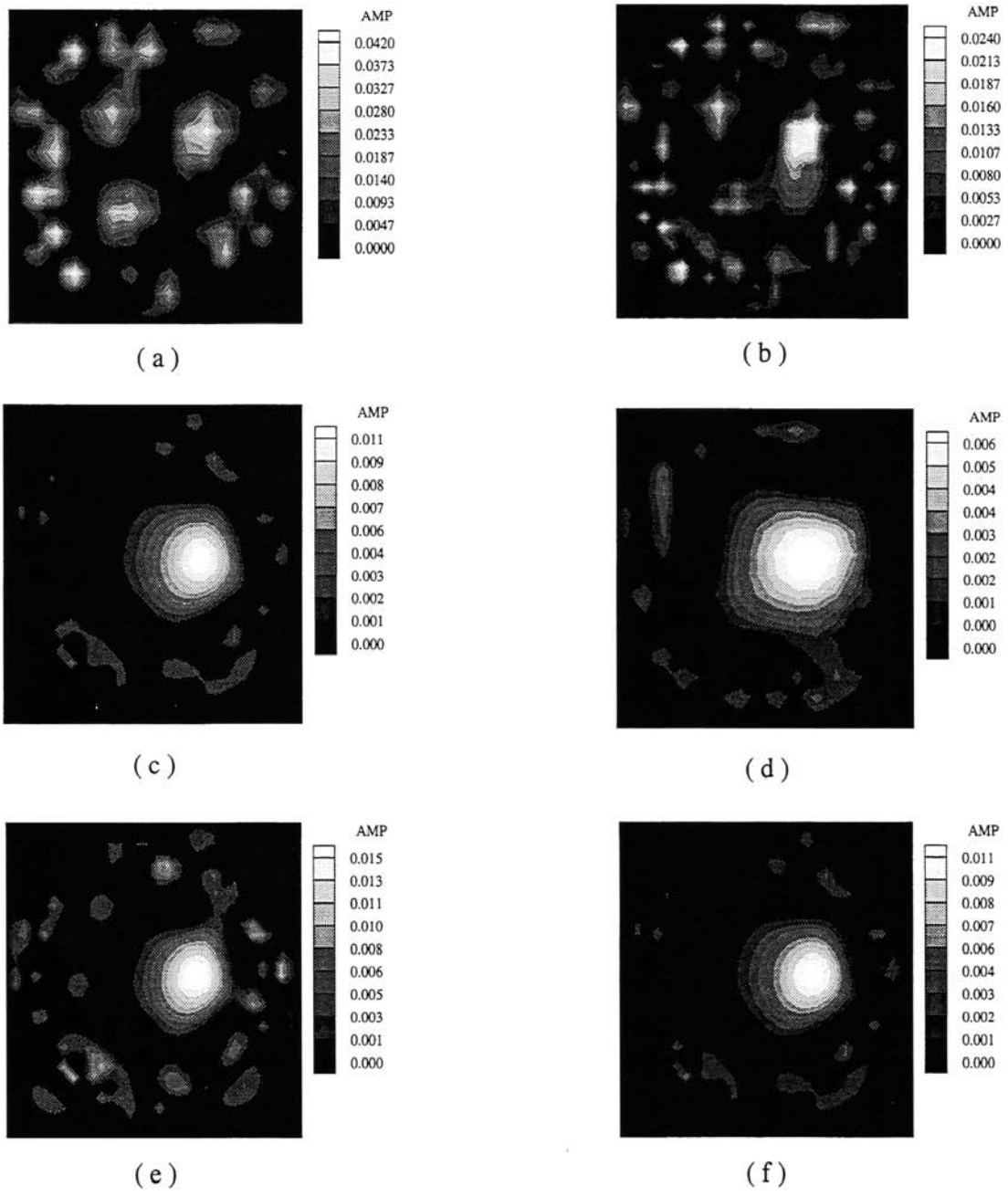

Figure 5: The reconstruction results for the medium shown in Fig. 4(a) when the data are corrupted by 10% noise. (a) is the reconstruction image with 500 iterations in the coarse grid without regularization; (b) is the reconstruction image with additional 200 iterations in the fine grid without regularization using (a) as an initial solution; (c) is the reconstruction image with additional 200 iterations in the fine grid with regularization also using (a) as an initial solution; (d) is the reconstruction image with 500 iterations in the coarse grid with regularization; (e) is the reconstruction image with additional 200 iterations in the fine grid without regularization using (d) as an initial solution; and (f) is the reconstruction image with additional 200 iterations in the fine grid with regularization using (d) as an initial solution.